Microbial Fuel Cell Using a Novel Ionic-Liquid-Type Membrane-Cathode Assembly with Heterotrophic Anodic Denitrification for Slurry Treatment

Adrián Hernández-Fernández [1] , Eduardo Iniesta-López [1] , Yolanda Garrido [1] , Ioannis A. Ieropoulos [2] and Francisco J. Hernández-Fernández [1,*]

[1] Department of Chemical Engineering, Faculty of Chemistry, University of Murcia (UMU), Campus de Espinardo, E-30100 Murcia, Spain; adrian.h.f@um.es (A.H.-F.); eduardo.iniestal@um.es (E.I.-L.); ygh46006@um.es (Y.G.)

[2] Civil, Maritime & Environmental Engineering Department, University of Southampton, Bolderwood Campus, Southampton SO16 7QF, UK; i.ieropoulos@soton.ac.uk

* Correspondence: fjhernan@um.es

Abstract: In this paper, microbial fuel cell technology with heterotrophic anodic denitrification, based on a new membrane-cathode assembly, was tested for slurry treatment and bioenergy production. Slurry is used due to its high chemical oxygen demand and a high content of nutrient compounds of nitrogen which can contaminate soil and water. The new membrane-cathode assembly systems were based on different ammonium and phosphonium cations combined with chloride, bistriflimide, phosphate, and phosphinate anions and a non-noble catalyst composed of copper and cobalt mixed-valence oxides. The influence of ionic liquids on the catalytic membrane was studied. The best membrane-cathode assembly was based on the ionic liquid catalyst [MTOA$^+$][Cl$^-$]-CoCu which achieved 65% of the energy reached with the Pt-Nafion® system. The [MTOA$^+$][Cl$^-$]-CoCu system improved the water purification parameter, reducing the COD by up to 35%, the concentration of nitrates by up to 26%, and the organic nitrogen by up to 70% during the experiments. This novel membrane-cathode system allows for easier manufacturing, lower costs, and simpler catalysts than conventionally used in microbial fuel cells.

Keywords: microbial fuel cell; ionic liquid; copper oxides; cobalt oxides; denitrification; slurry treatment

1. Introduction

Livestock farms are one of the most economically active sectors. The high demand for meat products has led to the development of intensive farms that generate large quantities of slurry. Untreated slurry can lead to contamination of the atmosphere and soil by nitrogenous compounds. This has made conventional slurry treatment infeasible and has motivated the scientific community and the business sector to look for new solutions for the treatment of slurry. Slurry is a mixture of approximately 40% faeces and 60% urine, with unconsumed feed material and water used for hygienic purposes. Farm slurry is characterised by a high biochemical and chemical oxygen demand (BOD and COD) and a high content of macronutrients, such as nitrogen, phosphorus, and potassium compounds [1]. Nitrogen is mainly found in the form of ammonium and organic nitrogen [2]. Organic nitrogen is converted into ammonium through the process of ammonification by heterotrophic bacteria. Ammonium in slurry can be biologically oxidised to nitrate, with nitrite as an intermediary. Nitrogen, in the form of nitrates, is easily washed out, reaching groundwater, rivers, and lakes, and most probably contributing to eutrophication [3]. In addition, ammonia and other compounds derived from untreated slurry are released into the atmosphere, significantly contributing to greenhouse gas emissions (N$_2$O, CH$_4$, and CO$_2$).

Microbial fuel cells (MFCs) are a new technology that makes it possible to convert the organic waste present in wastewater into electrical energy [4–7]. An MFC typically

comprises a cathode, an anode, and an ion-exchange membrane. Platinum (Pt) has been widely used as catalyst in the cathode to address sluggish reactions, but its high cost poses a barrier to commercialisation. Additionally, Pt is employed in the ion-exchange membrane, typically constructed from perfluorinated organic polymers [8]. While most research publications in the field of MFCs primarily focus on laboratory-scale applications, there is also a growing body of work related to pilot- or semi-industrial-scale applications. This shift in scale necessitates the exploration of more cost-effective materials compared to traditional options [9–11].

Recent research in this field has been centred on the development of novel nanostructured catalysts capable of matching platinum's reaction velocity. This is achieved by leveraging low-cost catalysts which are composed of non-noble metals, with the aim of paving the way for industrially viable technologies. Non-noble catalysts have been developed and tested for MFCs, including (i) MnO_2 [12], (ii) carbon [13,14], and (iii) biocathodes [15,16].

Ionic liquids (ILs) have emerged as an innovative immobilised phase in proton-exchange membranes. ILs are a class of salts that remain in a liquid state at or close to room temperature. They consist of organic cations, including common ones like ammonium, phosphonium, pyridinium, and imidazolium cations, paired with anions like chloride, hexafluorophosphate, and bistriflimide anions. ILs have garnered substantial attention due to their exceptional properties, such as high ionic conductivity, a broad electrochemical stability range, and thermal stability. They have been studied as alternative electrolytes for fuel cells, batteries, and sensors [17,18]. In the realm of MFCs, new generations of proton-exchange membranes based on ionic liquids have been employed, such as polymer ionic liquid inclusion membranes, also known as ionogels, based on ionic liquids [19].

Regarding the fuel in a microbial fuel cell, organic matter is oxidised by electrochemically active bacteria (EAB), while electrons produced by their metabolism pass from the anode to the cathode through an external electrical circuit. In the cathode, the electrons are transferred to an electron acceptor, such as oxygen [20]. MFCs can also integrate cathodic denitrification by microorganisms without energy input but coupled with anodic energy recovery for direct electron delivery. In these systems, nitrogen oxides act as electron acceptors to be reduced to nitrogen gas in the cathode, allowing simultaneous treatment of organic substrates in the anode chamber [21–23].

Nitrogen removal can also be carried out in the MFC using heterotrophic anodic denitrification (HAD). Drewnowski and Fernandez-Morales (2016) [24] found that HAD did not negatively affect the MFC power at low concentrations of nitrate in the influent. On the contrary, HAD can reduce energy recovery from the substrate at high concentrations of nitrate in the influent. Zhang et al. (2020) employed a dual-chamber microbial fuel cell (MFC) for the purpose of nitrogen removal. The cathode was responsible for ammonium oxidation and subsequent production of nitrate, which was then transported to the anode for heterotrophic denitrification (HAD) [25].

In this work, slurry purification using a heterotrophic anodic denitrification microbial fuel cell based on a new type of ionic liquid membranes was studied. Until now, MFCs based on ionic liquids used catalysts sprayed onto a carbon cloth [20]. In the new procedure described herein, the catalyst is suspended in the ionic liquid, which allows simpler manufacturing of the membrane–catalyst system, thus reducing costs. The power density, as well as COD reduction in the microbial fuel cells, was analysed, along with other physicochemical parameters such as BOD and nitrogen compounds. The influence of the nature of the ionic liquid in the membrane–catalyst system on the performance of the MFC was also studied.

2. Materials and Methods

2.1. Fuel and Chemicals

Slurry from the livestock farm of the Veterinary Faculty of the Universidad de Murcia was used as the fuel. The slurry also acted as a source of microflora to form the anodic bacterial community. The soluble chemical oxygen demand (COD) of the wastewater was 2286 mg/L. Polyvinylidene chloride, which was used to prepare the polymer inclusion membranes, was purchased from Sigma-Aldrich-Fluka (Darmstadt, Germany).

2.2. Ionic Liquids

The ILs studied were based on ammonium and phosphonium cations and were supplied by Sigma-Aldrich-Fluka Chemical Co. (Darmstadt, Germany) and IoLiTec (Heilbronn, Germany), and were of the highest purity available. Ionic liquids of different cation and anion compositions and different toxicities were tested. The ecotoxicity was measured as the inhibition ratio for *Saccharomyces cerevisiae* [26] and *Shewanella* sp. [27]. The higher the inhibition ratio, the higher the toxicity of the ionic liquids. Table 1 includes the full and abbreviated names of the ionic liquids used, their structures, and their chemical–physical properties.

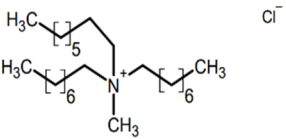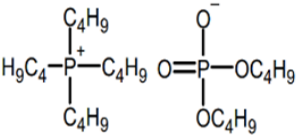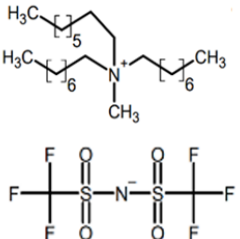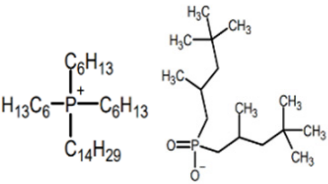### 2.3. Synthesis of Mixed-Valence Copper and Cobalt Oxides

$(Cu_{0.3}Co_{0.7})Co_2O_4$ was synthesised using the thermal decomposition method. In a previous investigation [28], copper-cobalt oxides with varying Cu:Co atomic ratios were prepared. Notably, the $(Cu_{0.3}Co_{0.7})Co_2O_4$ composition demonstrated the highest maximum power output in an MFC study [29].

The catalysts were synthesised using $CuCl_2$ and $CoCl_2$ as starting materials. Initially, copper and cobalt hydroxide ($CuOH_2$ and $CoOH_2$) co-precipitates were formed. This was achieved by slowly adding an excess of 3 M NaOH solution drop by drop into a mixture of the metal salt solutions ($CuCl_2$ and $CoCl_2$) at specified atomic ratios for Cu/Co-based oxides. The resulting mixture was stirred for 7 h at a temperature of 25 °C. After precipitation, the solid materials were separated from the solution through filtration and then thoroughly washed with deionised hot water. Subsequently, the wet precipitates were dried at 60 °C for 24 h using an oven. To obtain the final catalyst, the dried powder was subjected to heat treatment at temperatures ranging from 350 to 400 °C for 8 h. All chemicals used in this process were of reagent-grade quality and were procured from Sigma-Aldrich (Darmstadt, Germany).

The oxides were analysed for their crystallographic structure and purity using X-ray diffraction (XRD) carried out on a Bruker diffractometer (Bruker; Karlsruhe, Germany) equipped with a copper anode X-ray generator (X-ray Kristalloflex K 7608-80 F). Additionally, particle size measurements were performed using a JEOL JEM2100 transmission electron microscope (TEM).

The TEM images revealed the presence of copper-cobalt oxide nanoparticles, which exhibited dimensions ranging from 17 to 45 nanometres. Furthermore, the XRD patterns of the catalyst exhibited a cubic-packed spinel lattice structure, indicating a purity level of 100%, as determined by semi-quantitative analysis.

Table 1. Full and abbreviated names of the ionic liquids (ILs) analysed, and their structures and properties.

Full Name	Abbreviation	Structure	Water Miscibility	State at 25 °C	Radius of Inhibition (RI) (cm)
Methyltrioctylammonium chloride	$[N_{8,8,8,1}{}^{+}][Cl^{-}]$		Insoluble	Liquid	0.6 ± 0.2 [16] 3.0 ± 0.7 [17]
Tetrabutylphosphonium dibutyl phosphate	$[P_{4,4,4,4}{}^{+}][Bu_2Phos^{-}]$		Partially soluble	Liquid	0.5 ± 0.1 [16] 0.9 ± 0.2 [17]
Methyltrioctylammonium bis(trifluoromethylsulfonyl)imide	$[N_{8,8,8,1}{}^{+}][NTf_2{}^{-}]$		Insoluble	Liquid	0.0 [16] 1.2 ± 0.7 [17]
Trihexyl(tetradecyl)phosphonium bis 2,4,4-(trimethylpentyl)phosphinate	$[P_{6,6,6,14}{}^{+}][TMPPhos^{-}]$		Insoluble	Liquid	0.5 ± 0.1 [16] 2.6 ± 0.1 [17]

2.4. Preparation of New Proton-Exchange Membranes with Catalytic Activity Based on Ionic Liquids

The new membranes were obtained by casting methods using a PVC polymer and an ionic liquid. The amount of the ionic liquid in all cases was 70% *w/w* of the PVC/IL mixture. A mixture of IL (328 mg) with PVC (140 mg), Tetrahydrofuran (THF) (3 mL), and 15.6 mg of the catalyst was stirred for 10 min. The mixture was poured directly into a Fluka glass ring (28 mm inner diameter, 30 mm height) and onto a 3 cm diameter piece of carbon cloth (5% waterproof, Fuel Cell Earth, EEUU, Woburn, MA, USA) placed between the Fluka glass ring and a Fluka glass plate. This procedure resulted in the formation of a composite material known as IL/CuCo, consisting of a proton-exchange membrane, a catalyst, and a diffusion layer.

As a control (C), a Nafion® 117 proton-exchange membrane and a platinum cathode were used. The 15×15 cm Nafion® 117 sheets were purchased from Fuel Cell Earth, USA. Nafion® 117 must be pre-treated to activate the sulphonic acid group in its structure, replacing any positive ions that may have previously attached to the membrane with protons, using sulphuric acid. In this way, the activation protocol described in Pujiastuti and Onggo (2015) [30] was carried out. The Nafion® 117 membrane was immersed for 1 h in a 3% p/p hydrogen peroxide solution at 80 °C, then the membrane was immersed for 1 h in deionised water at 80 °C to remove any traces of H_2O_2, followed by 1 h in 1 M sulphuric acid solution at 80 °C. Finally, it was immersed for 1 h in deionised water at 80 °C. It was kept in a deionised water solution until use. As the catalyst, 60% platinum was used on a high-surface-area carbon support (HiSPEC® 9100, Alfa Aesar, Thermo Scientific, Waltham, MA, USA). The platinum mixture was sprayed onto a 3 cm diameter piece of waterproof carbon cloth 5% (Fuel Cell Earth, EEUU). The mixture was prepared by suspending the appropriate amount of platinum (6.3 mg of platinum or 10.5 of mixture Pt/C, 0.6 purity) in a 50/50 water/isopropanol solution, to which 20 μL of PTFE was added as a binder. The final load of platinum on the carbon cloth was 0.5 mg Pt cm^{-2}. The membrane and the platinum catalyst adsorbed on the piece of carbon cloth were fixed to the one-chamber reactor with a round joint clip (see Figure 1).
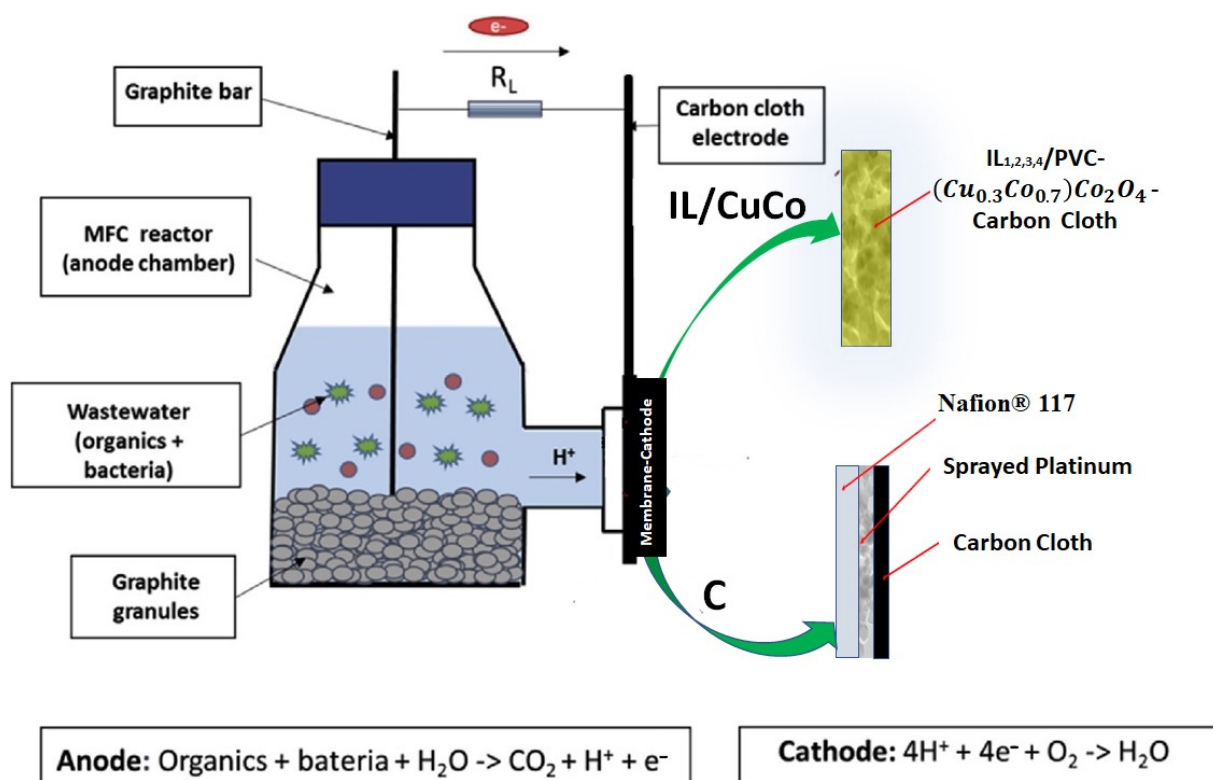

Figure 1. Schematic diagram of the reactor used in the experiments.

2.5. MFC Studies

New embedded membrane-cathode assemblies were implemented in one-chamber MFCs for slurry depuration and were evaluated in terms of their power output, COD reduction, and N removal. One-chamber MFCs of 250 mL were used for the experiments. The temperature was kept constant at 25 °C. The membrane-cathode assemblies used were those mentioned in the previous section ([$N_{8,8,1}^+$][Cl]/CuCo, [$P_{4,4,4,4}^+$][Bu$_2$Phos]/CuCo, [$N_{8,8,1}^+$][NTf$_2$]/CuCo, and [$P_{6,6,6,14}^+$][TMPPhos]/CuCo). Nafion$^®$/Pt were used as the membrane/cathode in the control assay (C). The anode in all cases consisted of 100 cm^3 of graphite granules of 2–6 mm diameter (Graphite Store, Northbrook, IL, USA) and a 3.18 mm diameter graphite rod (Graphite Store, USA) to connect to the cathode through a 1 kΩ resistor. The anode chambers were filled with 200 mL of feedstock. All reactors contained the membrane-cathode assembly at the end of the cylindrical flange. The membrane-cathode system was attached to the end of the reactor flange with a round joint clip. All experiments were conducted using a batch mode approach, utilising wastewater as the sole source of microorganisms and fuel. Two replicates were made for each of the experimental conditions.

The experiments were always started with a clean anode, the anode was filled with wastewater and the biofilm developed on the anode surface (maturation period). After the maturation period, the wastewater was changed, and the depuration experiment was started. The total duration of the test was 312 h. The first polarisation test was carried out about 24 h after the beginning of each experiment. Then, polarisation tests were performed at 48 h, 72 h, 144 h, and 312 h to study the evolution of the MFC performance over time.

2.6. Analytical Methods

2.6.1. Chemical Analysis

The fuel was characterised during wastewater depuration from the point of view of its purification in terms of COD (chemical oxygen demand), total nitrogen (organic and inorganic nitrogen), nitrates (NO$_3^-$), nitrites (NO$_2^-$), ammoniacal nitrogen (NH$_4^+$, NH$_3$), and BOD$_5$ (biochemical oxygen demand at 5 days), among others. Wastewater samples were taken periodically. The samples were previously filtrated with 0.45 nm nylon syringe filters (Fisherbrand-Fisher Scientific, Waltham, WA, USA). As needed, the samples underwent digestion using a TR 420 thermoreactor for Spectroquant from Merck Millipore (Darmstadt, Germany). The chemical composition analysis of these samples was conducted via spectrophotometry, utilising the SpectroQuant Prove 300 apparatus from Merck Millipore, in conjunction with specialised kits. The following methods were applied:

- Chemical oxygen demand (COD) tests were conducted using COD 145,541 Supelco cuvettes from Sigma-Aldrich, following the procedure outlined in DIN ISO 15705. This method has received approval from the USEPA for wastewater analysis.
- Total nitrogen (organic and inorganic nitrogen) tests were conducted in nitrogen (total) 114,763 Supelco cuvettes (Sigma-Aldrich). The digestion is analogous to EN ISO 11906-1.
- Nitrates (NO$_3^-$) tests were conducted in nitrates 100,614 Supelco cuvettes (Sigma-Aldrich). The procedure is analogous to DIN 38405-9.
- Nitrites (NO$_2^-$) tests were conducted in nitrites 114,547 Supelco cuvettes (Sigma-Aldrich). The procedure is analogous to EPA 354.1, APHA 4500-NO2 B, DIN EN 26 777, and ISO 6777.
- Ammoniacal nitrogen (NH$_4^+$, NH$_3$) tests were conducted in ammonium 114,559 Supelco cuvettes (Sigma-Aldrich). The procedure is analogous to EPA 350.1, APHA 4500-NH3 F, ISO 7150-1, and DIN 38406-5.
- Biochemical oxygen demand at 5 days (BOD$_5$) was determined. A system of six Velp Scientifica instruments was employed for the manometric assessment of BOD. In this process, dicyanamide served as an inhibitor for nitrification.

2.6.2. Electrochemical Analysis

To analyse the electric performance of the new materials, polarisation tests were carried out and the internal resistance was calculated.

Polarisation Test

The voltage was continuously monitored using a data acquisition system (PCI 6010, National Instruments, Austin, TX, USA) at a scan rate of one data point per minute. At intervals, readings were taken offline using a DVM891 digital multimeter manufactured by HQ Power in Germany. Polarisation measurements were conducted utilising a variable resistor box with a range of resistance values, including 5.77 MΩ, 953 kΩ, 486 kΩ, 96.5 kΩ, 50 kΩ, 11 kΩ, 6 kΩ, 1.1 kΩ, 561 Ω, 94.5 Ω, and 1.5 Ω.

The voltage value in each case was taken once the cell had reached the pseudo-steady state under the corresponding resistor value; the average time to reach the pseudo-steady state was taken as 1 min.

Internal Resistance

The internal resistance $R_{int}(\Omega)$ of each MFC was calculated from Equation (1):

$$R_{int}(\Omega) = \frac{OCV\ (V)}{I(A)} - R_{ext}(\Omega) \tag{1}$$

where $OCV\ (V)$ represents the open circuit voltage, $I(A)$ denotes the current density at peak power, and $R_{ext}(\Omega)$ stands for the external resistance at peak power.

2.7. Statistical Analysis

The data were analysed using PASW Statistics 28 for Windows (SPSS Inc., Chicago, IL, USA). The Student's *t*-test with a significance level at $p < 0.05$ was performed to compare the different treatments analysed. Values are the mean $\pm$ standard deviation of two replicates.

2.8. SEM-EDX Characterisation

A scanning electron microscope (SEM, APREO S) and AXS analyser for energy-dispersive X-ray (EDX, JEOL-6100) were used to study the appearance and chemical composition of the membrane-cathode assembly systems. They were characterised after preparation (fresh) and after operation in the MFCs.

3. Results and Discussion

3.1. Electrochemical Analysis

Initially, 200 mL of slurry was added to form a biofilm around the graphite granules (maturation period). The MFC voltage with different membrane-cathode systems was continuously monitored for more than 100 h with a 1 kΩ external resistor during the maturation period. During the first period of 96 h the voltage increased until a plateau was reached of 201 mV for Nafion®/Pt, 159 mV for [N$_{8,8,8,1}^+$][Cl$^-$]/CuCo, and 6 mV for [N$_{8,8,8,1}^+$][NTf$_2^-$]/CuCo. When the maximum voltage was reached or the voltage stabilised during the maturation period, the residual water was changed, and the depuration experiment was started. The voltage profiles of the different depuration experiments over time are shown in Figure 2. As expected, in the depuration experiments, the maximum voltage was reached faster when compared to the maturation period, since the biofilm around the graphic granules had already been created.
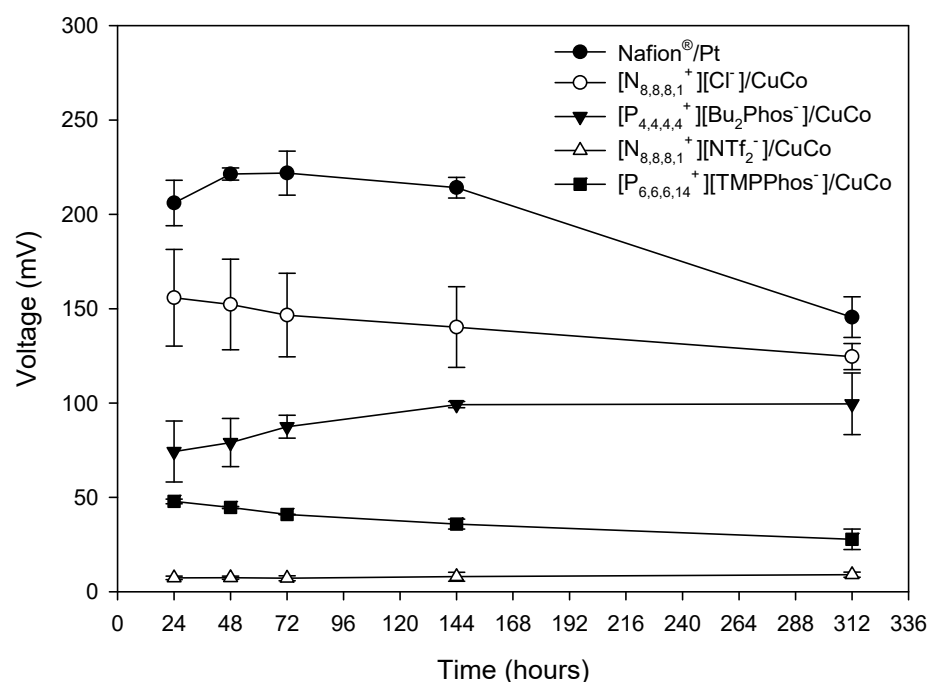
Figure 2. Voltage output under 1 kΩ external resistance during the depuration experiment for different embedded membrane-cathode assembly systems ($N_{8,8,8,1}^+$)[Cl$^-$]/CuCo, [$P_{4,4,4,4}^+$][Bu$_2$Phos$^-$]/CuCo, [$N_{8,8,8,1}^+$][NTf$_2^-$]/CuCo, and [$P_{6,6,6,14}^+$][TMPPhos$^-$]/CuCo) and control (Nafion®/Pt) working in batch mode. Mean values and standard deviations are shown in the figure.

As shown in Figure 1, the Nafion®/Pt control system produces the highest voltage over time, as expected, but the good performance of the [$N_{8,8,8,1}^+$][Cl$^-$]/CuCo system, which reaches values of around 71% of the control, is noteworthy.

Polarisation curves were obtained at 24 h, 48 h, 72 h, 144 h, 192 h, and 312 h by varying the resistance between the two electrodes and determining the voltage and intensity produced. As an example, Figure 3A shows the polarisation curves for [$N_{8,8,8,1}^+$][Cl$^-$]/CuCo, [$P_{4,4,4,4}^+$][Bu$_2$Phos$^-$]/CuCo, [$N_{8,8,8,1}^+$][NTf$_2^-$]/CuCo, and [$P_{6,6,6,14}^+$][TMPPhos$^-$]/CuCo and Nafion®/Pt at 24 h. Polarisation curves at 48 h, 72 h, 144 h, and 192 h are included in Appendix A (Figures A1–A4).

Figure 3A shows the maximum value of OCV for Nafion®/Pt at 512 mV. [$N_{8,8,8,1}^+$][Cl$^-$]/CuCo and [$P_{4,4,4,4}^+$][Bu$_2$Phos$^-$]/CuCo showed the maximum value of OCV at 424 and 360 mV, respectively. The lowest OCV values were found for [$P_{6,6,6,14}^+$][TMPPhos$^-$]/CuCo and [$N_{8,8,8,1}^+$][NTf$_2^-$]/CuCo, being 316 and 155 mV, respectively. Polarisation curves also provide information on the electrochemical behaviour of the system. At lower densities, the curve's shape is associated with the activation energy of the electrode reaction. This is followed by a linear segment where the microbial fuel cell (MFC) adheres to Ohm's law, with the system's limiting step being the charge transfer through the system. Toward the end of the curve, if linearity is lost once more, it signifies that mass transport becomes the limiting step. In a first stage, for low current densities, all of the ionic liquid systems show an exponential voltage loss curve. The exponential voltage loss is much lower in the case of the Nafion®/Pt system, resulting in a lower activation loss. At medium current densities, a linear decrease in voltage over intensity is observed due to ohmic losses. In the case of Nafion®/Pt and [$N_{8,8,8,1}^+$][Cl$^-$]/CuCo, the slopes of the linear sections of their polarisation curves are not as steep due to the lower internal resistance of these systems compared to the other IL/CuCo systems. At high current densities, no mass transfer loss is observed in the polarisation curve. One of the advantages of single-chamber MFCs is that oxygen mass transfer losses are minimal or non-existent as the cathode is exposed to air.

The limiting current densities range from 1600 mA m^{-2} for Nafion®/Pt to 50 mA m^{-2} for [P$_{6,6,6,14}$$^+$][TMPPhos$^-$]/CuCo.
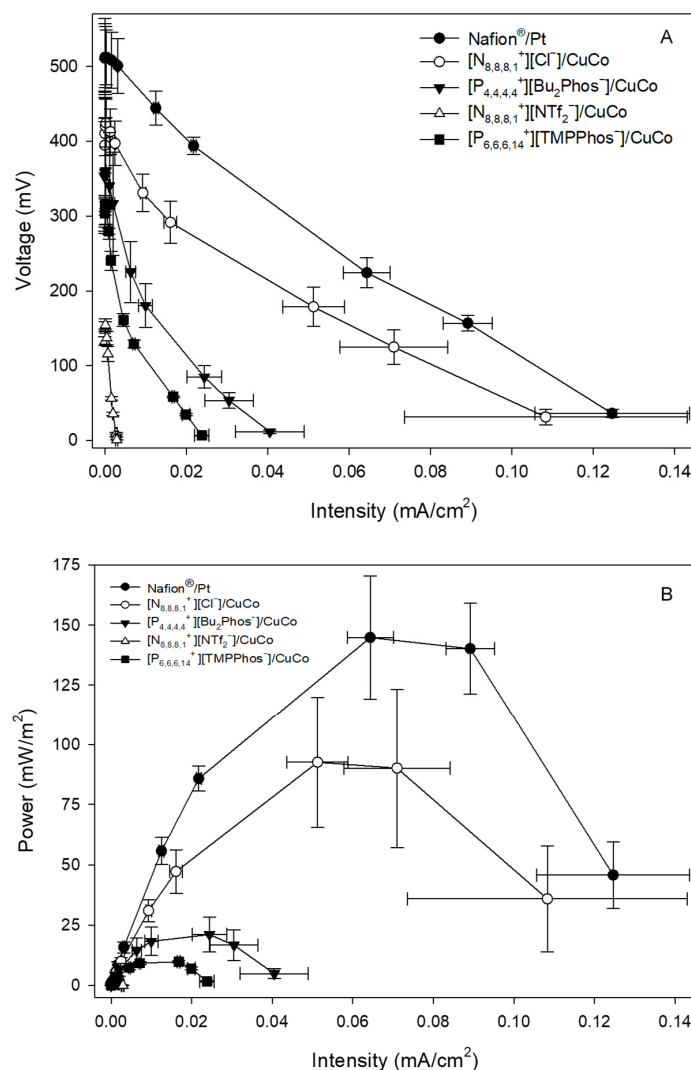

Figure 3. Polarisation (**A**) and power (**B**) curves of MFCs with different embedded membrane-cathode assembly systems at 24 h. Calculations are based on the surface of the membrane-cathode assembly.

The power output curves of the different membrane-cathode assembly systems are shown in Figure 3B. In almost all of the systems, the maximum power is reached in the range of 560 Ω to 1110 Ω. As can be seen in Figure 3B, the Nafion®/Pt system (C) generates the highest power, with a maximum power of 145 mWm^{-2}, followed by the [N$_{8,8,8,1}$$^+$][Cl$^-$]/CuCo system, which presents a maximum power of 93 mWm^{-2}, which represents a power value that is 64% of that of the Nafion®/Pt control. The maximum power for the rest of systems follows the sequence: [P$_{4,4,4,4}$$^+$][Bu$_2$Phos$^-$]/CuCo (20%C) > [P$_{6,6,6,14}$$^+$][TMPPhos$^-$]/CuCo (6%C) > [N$_{8,8,8,1}$$^+$][NTf$_2$$^-$]/CuCo (0.6%C). Kiely et al. [31] utilised an air cathode microbial fuel cell. The cathode was constructed by applying platinum at a loading of 0.5 mg/cm^2 and four diffusion layers made of polytetrafluoroethylene (PTFE) onto carbon cloth. They employed dairy manure wastewater with a COD concentration of 450 mg/L. Their research findings indicated that they achieved a maximum power density of 189 mW/m^2.

Polarisation curves were also recorded over time at 48 h, 72 h, 144 h, 192 h, and 312 h. The trends mentioned above for the polarisation curve at 24 h were confirmed for the polarisation curves at different times. Figure 4 shows the variation in the maximum potential, obtained from the polarisation curves, over time. A decrease in the maximum power

reached over time was observed for the systems with higher power, (Nafion®/Pt) and [N$_{8,8,8,1}^+$][Cl$^-$]/CuCo, which is related to the decrease in the residual water concentration over the 312 h of testing. It is important to note that the differences observed between the Nafion®/Pt system (Nafion-Pt) and the [N$_{8,8,8,1}^+$][Cl$^-$]/CuCo system decreased over time.
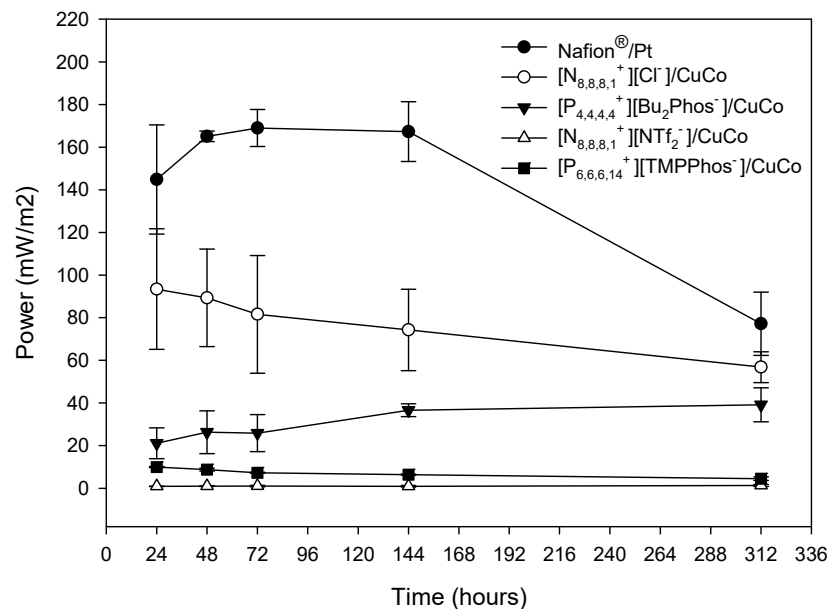

Figure 4. Maximum power over time, obtained from the polarisation experiments, during the depuration experiment for different embedded membrane-cathode assembly systems and the control system (Nafion®/Pt) working in batch mode. The mean values and standard deviation are shown in the figure.

The polarisation curves also allow the calculation of the approximate internal resistance. The internal resistance is a parameter that influences the capacity of the different systems to produce electricity. In MFCs, it is related to diffusion limitations and structural barriers, which entails energy losses. In our systems, the different internal resistance is mainly related to the different membrane-cathode compositions. Figure 5 shows the internal resistance for different membrane–catalyst systems over time. The control (C), which was composed of Nafion® and Pt, showed the lowest internal resistance (over 1033 Ω), which remained the same over time. Consequently, the highest maximum power was obtained for the Nafion®/Pt system. The IL$_1$ resistance (1203 Ω) is similar to that of the control system. Higher internal resistance values were obtained for the other IL/CuCo systems. It is important to note that this resistance remains constant over time for the control, [N$_{8,8,8,1}^+$][Cl$^-$]/CuCo, and [P$_{4,4,4,4}^+$][Bu$_2$Phos$^-$]/CuCo, which implies a stability of the membrane during the experiment.

To understand the relationship between the composition of the ionic liquids and their activity in the integrated cathode-membrane systems in MFCs, we will consider the properties of the ionic liquids represented in Table 1. It can be concluded that there is no close relationship between the ecotoxicity of the ionic liquid and the maximum power of the MFC, as the ionic liquids that showed the highest radius of inhibition (i.e., [N$_{8,8,8,1}^+$][Cl$^-$]) presented the highest maximum power. In relation to this issue, it should also be noted that the ionic liquids selected for this application are very insoluble and, moreover, they are entrapped as ionogels, which makes their release from the membrane-cathode assembly difficult. Therefore, if a small amount of ionic liquids was released from the membrane-cathode assembly, the concentration of ionic liquids in the medium would be below ecotoxic concentrations for the microorganisms present in the anode.
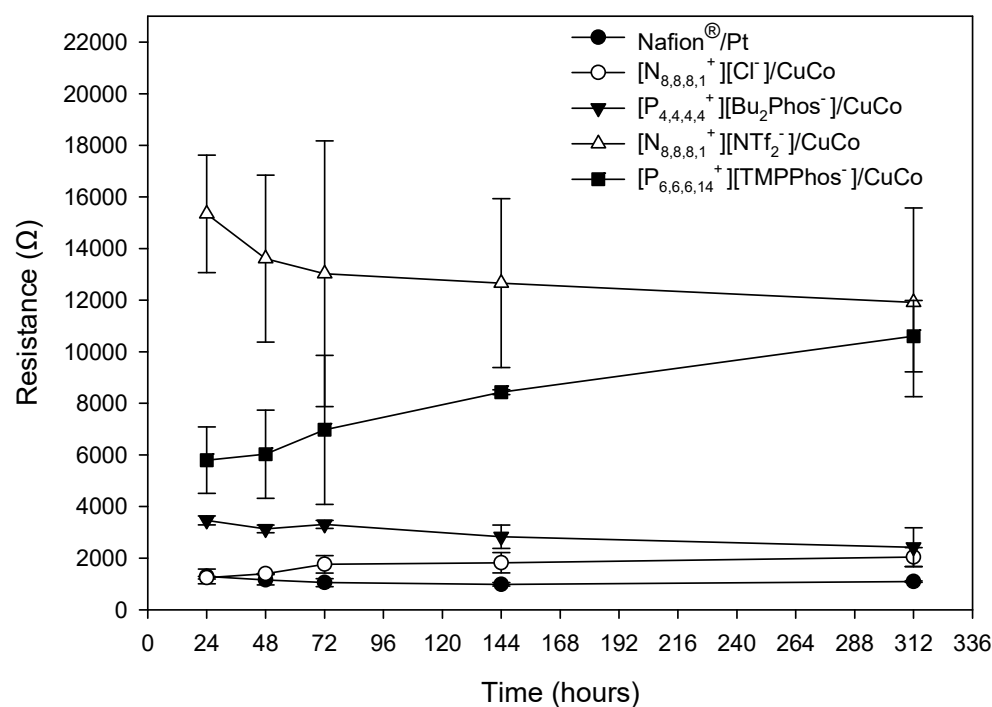
Figure 5. Internal resistance values over time, obtained from the polarisation experiments, during the depuration experiment for the different embedded membrane-cathode assembly systems and control system (Nafion®/Pt) working in batch mode. The mean values and standard deviation are shown in the figure.

Furthermore, a low viscosity does not significantly affect the action of ionic liquids as proton exchangers by diffusion through the membrane, since the power values using the chloride-based ionic liquid were higher than those obtained for the bistriflimide-based ionic liquid, which has a lower viscosity than the chloride ionic liquid. It is important to note that the degree of hydration of the ionic liquid $[N_{8,8,8,1}{}^+][Cl^-]$ is higher than that of the ionic liquid $[N_{8,8,8,1}{}^+][NTf_2{}^-]$ as the latter is more hydrophobic. This fact could affect the viscosity of $[N_{8,8,8,1}{}^+][Cl^-]$ and its capacity to transport protons. On the other hand, the chloride anion has a more localised charge than the bistriflimide anion, which could improve the interaction with cations such as protons and, thus, the transport of protons and the power of the MFC. The higher charge density of chloride may also facilitate interaction with water and, consequently, hydration of the ionic liquid. All these design factors are currently being studied in more detail in our laboratories.

Furthermore, it is very important to note that the most common methodology for cathode preparation is based on the spraying of Pt/C, water, isopropanol, and PTFE [32,33]. The new methodology is simpler than the conventional one and is based on a mixture of the ionic liquid phase, the catalyst, and a plasticiser that acts as a membrane/catalyst composite material. Using this new technique, and the procedure for obtaining the $[N_{8,8,8,1}{}^+][Cl^-]$/CuCo membrane-cathode system, very good results were obtained compared to the conventional Nafion®/Pt system. The new preparation technique is much easier to mechanise if we intend to prepare industrial cathodes.

3.2. Slurry Wastewater Treatment Using Microbial Fuel Cells

Since the possibility of using complex substrates was discovered, different wastewaters have been tested in MFCs to demonstrate the feasibility of this technology for water treatment [34–36]. Slurry wastewater has been chosen because of the high environmental problem it generates due to its high organic load and high nutrient content, as discussed above. The physicochemical characteristics of slurry wastewater can be seen in Table 2.

Table 2. Chemical composition of the slurry wastewater before and after 312 h of treatment (as % reduction) with the different MFC technologies. [COD]: Chemical oxygen demand. [NO_2-N]: concentration of nitrites. [NO_3-N]: concentration of nitrates. [NH_4-N]: concentration of Ammoniacal nitrogen. [N_T]: Total nitrogen. [$N_{organic}$]: concentration of organic nitrogen.

Parameter	Initial Values (mg/L)	Nafion®/Pt (%)	[$N_{8,8,8,1}^+$][Cl^-]/CuCo (%)	[$P_{4,4,4,4}^+$][Bu_2Phos^-]/ CuCo (%)	[$N_{8,8,8,1}^+$][NTf_2^-]/Cu Co (%)	[$P_{6,6,6,14}^+$][TMP-Phos$^-$]/CuCo(%)
[COD]	2286 ± 5.66	53.46 ± 3.47	35.33 ± 11.79	23.03 ± 21.16	38.83 ± 11.41	32.67 ± 3.45
[NO_2-N]	0.104 ± 0.02	0 ± 12.05	10.57 ± 4.34	14.51 ± 12.48	6.89 ± 1.5	1.78 ± 5.73
[NO_3-N]	5.25 ± 0.64	12.01 ± 9.54	26.64 ± 15.35	17.27 ± 2.09	14.64 ± 5.82	3.12 ± 4.42
[NH_4-N]	622 ± 24.04	2.6 ± 2.51	0 ± 2.01	2.79 ± 5.35	0 ± 1.93	0 ± 6.65
[N_T]	680 ± 14.14	9.51 ± 5	3.64 ± 3.04	5.8 ± 8.2	2.13 ± 7.23	0.75 ± 1.06
[$N_{organic}$]	52.65 ± 10.56	96.68 ± 56.5	70.03 ± 32.71	45.26 ± 52.03	69.96 ± 86.96	15.59 ± 87.82

Values are the mean ± standard deviation of two replicates.

Chemical oxygen demand (COD) was one of the parameters used to measure the slurry treatment capacity of the microbial fuel cells. The initial COD of the slurry wastewater sample was determined to be 2286 mg/L. The evolution of this parameter was also determined over the test time (312 h) for the different types of microbial fuel cells (Nafion®/Pt, [$N_{8,8,8,1}^+$][Cl^-]/CuCo, [$P_{4,4,4,4}^+$][Bu_2Phos^-]/CuCo, [$N_{8,8,8,1}^+$][NTf_2^-]/CuCo, and [$P_{6,6,6,14}^+$][TMPPhos$^-$]/CuCo) (see Figure 6). The percentages of COD reduction in each MFC are shown in Figure 6.

COD removal increased during all experiments. After 300 h, the COD reduction was 54% for the Nafion®/Pt system, 23% for the [$P_{4,4,4,4}^+$][Bu_2Phos^-]/CuCo system, and around 35% for the other membrane-cathode assembly systems. In the case of the [$P_{4,4,4,4}^+$][Bu_2Phos^-]/CuCo system, a significantly lower COD reduction was observed, which may be because this ionic liquid is partially soluble in the aqueous phase, which could increase the COD value.
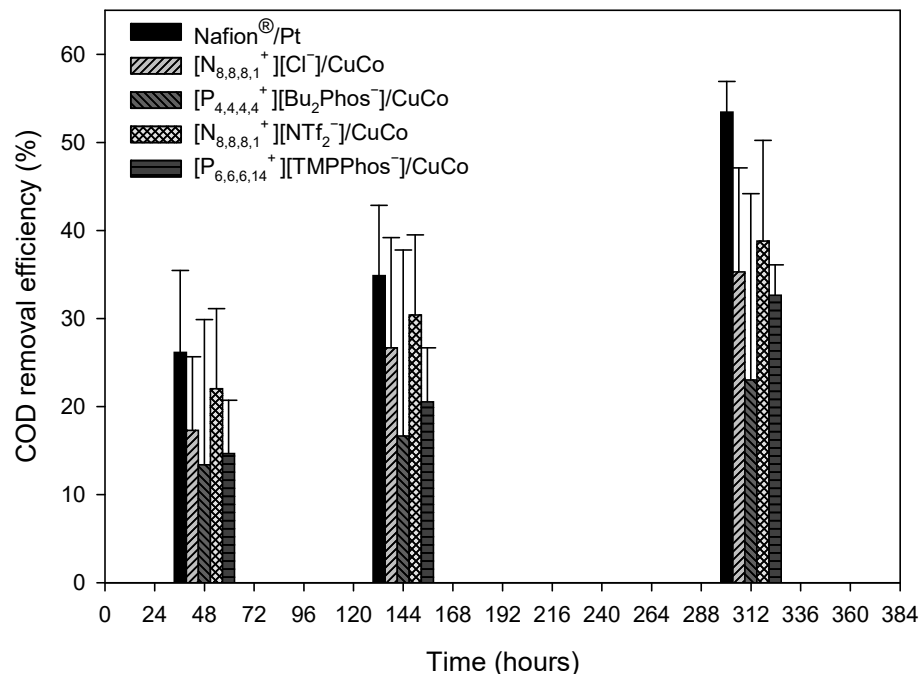

Figure 6. COD removal yields at different times for the Nafion®/Pt control system and the IL_1, IL_2, IL_3, and IL_4 systems.

It is worth noting that there is a scarcity of research in the literature that delves into the utilisation of slurry as a fuel source in microbial fuel cells. Furthermore, previous studies typically involved slurry with significantly lower COD levels than the one employed in our research. For instance, in the study conducted by Yokohama et al. [37], they investigated the purification of a slurry containing faeces and urine from Holstein cows using cathode-

in-air microbial fuel cells. Their cathode featured a platinum catalyst with a loading of 0.5 mg/cm^2, which was attached to a Nafion-115 proton-exchange membrane. Initially, the chemical oxygen demand (COD) values in the slurry stood at 1010 mg/L, and their research demonstrated an approximate 71% reduction in COD within a 70 h timeframe. Their maximum power density was approximately 0.34 mW/m^2. The lower COD reduction in our sample may be attributed to the elevated ammonium concentration. Our wastewater initially contained approximately 622 mg/L of ammonium, whereas in the prior study it was around 38.9 mg/L. Therefore, the lower COD reduction in our MFC could be correlated with a higher ammonium content, which is known to be toxic and can impede the degradability of organic matter.

In contrast, our system exhibited a lower limit for the maximum power density of approximately 50 mW/m^2, with the highest value being around 225 mW/m^2.

Regarding the elimination of the different forms of nitrogen, the initial and final values are presented in Table 2. General behaviours can be observed that are helpful when analysing the technology of microbial fuel cells. In all systems except the control system, there was a reduction in nitrite and nitrate forms in the feed water. This can be explained by the fact that under anoxic conditions in the anode, denitrifying bacteria use nitrate as an electron acceptor. In some systems, such as $[N_{8,8,8,1}^+][Cl^-]$/CuCo, reductions of up to 26% of NO_3^- can occur. In all cases, a decrease in total and organic nitrogen was observed, the highest values being close to 10% and 96%, respectively, for the control system. The increase in ammoniacal nitrogen observed for some systems can be explained by the mineralisation of organic hydrogen in the anode. The $[N_{8,8,8,1}^+][Cl^-]$/CuCo and $[N_{8,8,8,1}^+][NTf_2^-]$/CuCo systems, which contain an ammonium cation, could influence the total nitrogen value, as some of these ionic liquids could be released from the surface membrane despite their low solubility. Yokohama et al. [37] also studied the total nitrogen and ammoniacal nitrogen, and they found a reduction of 16% for total nitrogen and the ammoniacal nitrogen was increased after treatment.

When analysing the data, we must consider that the great variability obtained in some cases, as indicated by the statistical values of the parameters, is mainly due to two different reasons: (i) microbial fuel cells are very complex systems with high variability, even when performing repeated tests under identical conditions [38]; and (ii) the low concentration of some chemical compounds (like the oxidised forms of nitrogen) in the microbial fuel cell system.

3.3. Characterisation of Membrane–Catalyst Assembly Systems

The best membrane–catalyst assembly system, $[N_{8,8,8,1}^+][Cl^-]$-CuCo, was characterised using SEM-EDX techniques. Figure 7 shows SEM micrographs of the membrane assembled to the cathode ($[N_{8,8,8,1}^+][Cl^-]$-CuCo) on the side in contact with the anodic solution before testing and after more than 300 h of testing. Figure 7 shows the air side after operation.
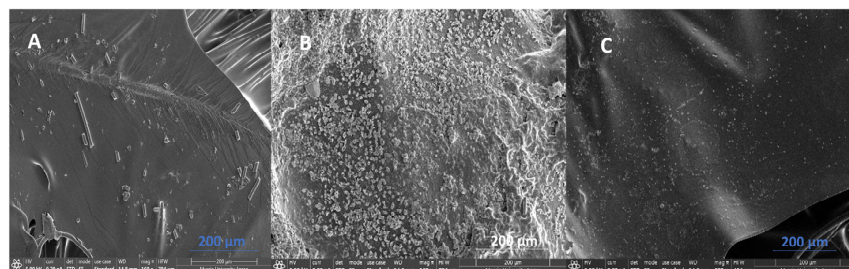

Figure 7. Scanning electron micrographs of the membrane–catalyst assembly system $[N_{8,8,8,1}^+][Cl^-]$-CuCo, 30% PVC, and $(Cu_{0.3}Co_{0.7})Co_2O_4$ (200 μm scale, blue double-headed arrow). (**A**) Anodic solution side before operation; (**B**) anodic solution side after operation; and (**C**) air side after operation.

Figure 7A shows a relatively homogeneous surface, with some roughness, grooves, and filaments attributed to the carbon fibre. After the use of the catalytic membrane, some

deposits appear on the surface (see details in Figure 7B). In Figure 7C, we can observe the SEM micrograph of the side exposed to air after 300 h of operation. This side exhibits a greater degree of uniformity compared to the opposite side, which is in contact with the anodic solution (Figure 7B). Furthermore, there are no deposits visible on its surface.

EDX spectra of the membrane-cathode assembly were performed after and before operation. Table 3 provides a summary of the elemental peaks in atomic percentage (%) based on the EDX spectra of the PEM-catalyst assembly, utilising [MTOA$^+$][Cl$^-$] ionic liquids, 30% PVC, and $(Cu_{0.3}Co_{0.7})Co_2O_4$. It is important to note that the EDX spectra were obtained from a sample with a thickness/depth of only a few micrometres, which means that the analysis pertains to the surface of the catalytic membrane.

Table 3. Peak element vs. atomic % for EDX spectra of PEM-catalyst assembly based on [N$_{8,8,8,1}^+$][Cl$^-$] ionic liquids, 30% PVC, and $(Cu_{0.3}Co_{0.7})Co_2O_4$. A: Anodic solution side before operation; B: anodic solution side after 300 h operation; and C: air side after 300 h operation.

PEM-Catalyst Assembly ([MTOA$^+$][Cl$^-$]-PVC-($Cu_{0.3}Co_{0.7}$)Co_2O_4)-Carbon Cloth			
Peak Element	**Atomic % A**	**Atomic % B**	**Atomic % C**
C K	87.16	65.8	76.21
N K	-	-	-
O K	-	22.69	3.17
Cl K	13.29	11.02	20.82
Ca K	-	8.09	-
Co K	0.22	0.15	0.79
Cu K	0.10	-	0.15
Pt M	0.37	0.68	0.70

Furthermore, it should be considered that EDX is a semi-quantitative technique; however, it is a very powerful technique that provides a lot of information.

The EDX spectra of the membrane-cathode assembly always showed the characteristic peaks assigned to Cu and Co K, demonstrating the stability of the catalyst on the membrane surface after operation. The EDX spectra showed the presence of Ca salt (Ca K peaks) on the side of the catalyst membrane in contact with the anode solution after operation due to salt deposits on the membrane. The platinum M peak was observed due to the need to coat the sample with platinum in the technique used. The nitrogen K peaks were very small due to the technique being very sensitive to the molecular weight of the atom analysed. The presence of the ionic liquid [N$_{8,8,8,1}^+$][Cl$^-$] could be determined due to the atomic % of Chloride in the sample. The theoretical atomic % for Cl in [N$_{8,8,8,1}^+$][Cl$^-$] is 3.7% (without considering H, which does not appear in EDX spectra), and the theoretical atomic % for Cl in PVC (C_2H_3Cl) (without considering H) is 33.3%. Therefore, the atomic Cl % content should be between 3.7% and 33.3% in the mixture of the ionic liquid/PVC. In fact, in all cases the chloride atomic % of chloride was within this range. However, in the air side (C), the Cl atomic % was increased and approached the % of free PVC. As previously noted, EDX provides insights into the composition of the membrane's surface within the first few micrometres. Keeping this in mind, it can be inferred that the ionic liquid had undergone some degree of rinsing. The choice of ionic liquids (specifically, [N$_{8,8,8,1}^+$][Cl$^-$]) was made with consideration of their low solubility in water (<0.02% (*v/v*)), aimed at enhancing the membrane's stability in aqueous solutions. Furthermore, the use of the occlusion method with PVC has been demonstrated to further bolster the stability of the liquid membrane in aqueous environments [39].

4. Conclusions

In this work, a microbial fuel cell technology based on a new type of membrane-cathode systems based on ionic liquids was studied. Slurry was used as the fuel due to its high organic matter and high concentration of nitrogen compounds, which are able to contaminate soil and water. The new membrane-cathode assembly system was based

on different ammonium and phosphonium cations combined with chloride, bistriflimide, phosphate, and phosphinate anions and a non-noble catalyst composed of copper and cobalt mixed-valence oxides. The best membrane-cathode assembly was the $[N_{8,8,1}^+][Cl^-]$-CuCo system based on the ionic liquid $[N_{8,8,1}^+][Cl^-]$. With this ionic liquid the power reaches 65% of the Nafion®/Pt system's power. The localised negative charge of chloride of this ionic liquid with respect to other anions looks like a key factor in favouring the higher proton conductivity and, consequently, the power of the microbial fuel cell. The $[N_{8,8,1}^+][Cl^-]$-CuCo system also reduces the COD by 35%, the concentration of nitrates by 26%, and the organic nitrogen by 70%.

The novel membrane-cathode composite materials allow for easier manufacturing and cheaper membranes and catalyst than the conventional ones used in microbial fuel cells.

Author Contributions: Conceptualisation, F.J.H.-F., I.A.I. and A.H.-F.; methodology, A.H.-F., E.I.-L. and Y.G.; formal analysis, F.J.H.-F. and I.A.I.; software, A.H.-F. and E.I.-L.; investigation, A.H.-F., E.I.-L. and Y.G.; data curation, A.H.-F., E.I.-L. and Y.G.; writing—review and editing, F.J.H.-F., I.A.I. and A.H.-F.; supervision, F.J.H.-F. and I.A.I.; project administration, F.J.H.-F.; funding acquisition, F.J.H.-F. All authors have read and agreed to the published version of the manuscript.

Informed Consent Statement: Not applicable.

Data Availability Statement: Data are available under reasonable request.

Conflicts of Interest: The authors declare no conflict of interest. The funders had no role in the design of the study; in the collection, analyses, or interpretation of data; in the writing of the manuscript; or in the decision to publish the results.
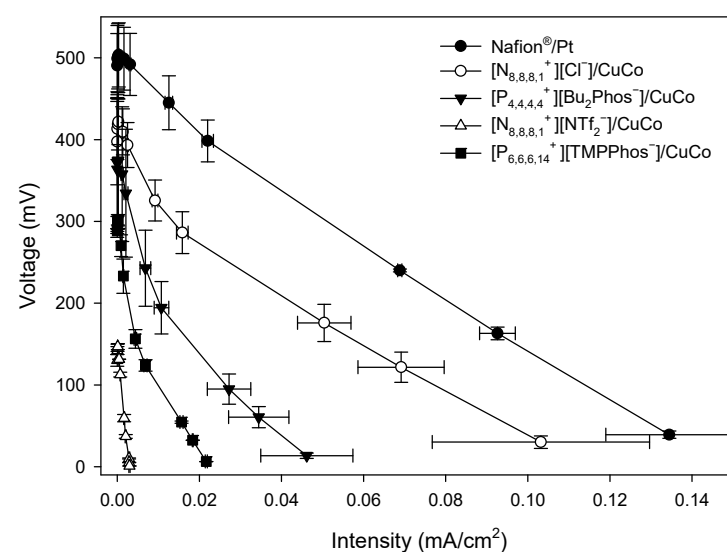
Appendix A

Figure A1. Polarisation curves of MFCs with different embedded membrane-cathode assembly systems at 48 h.
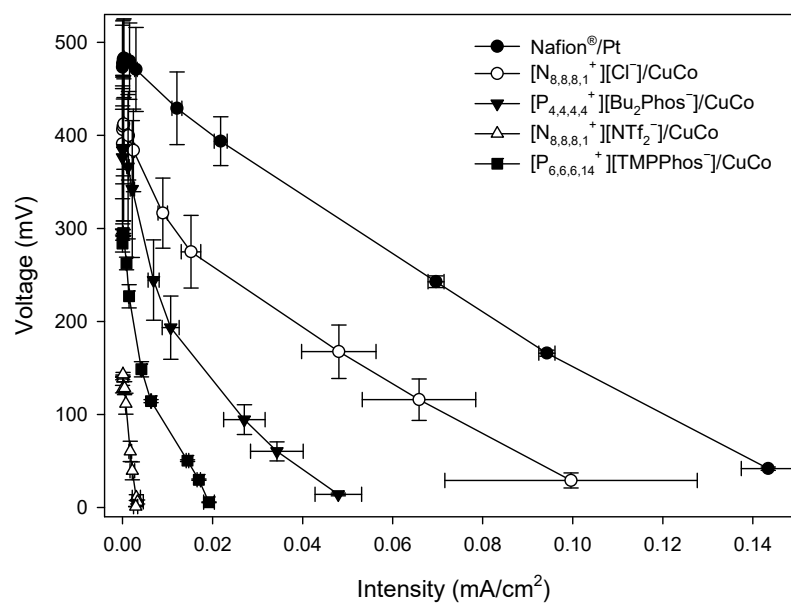
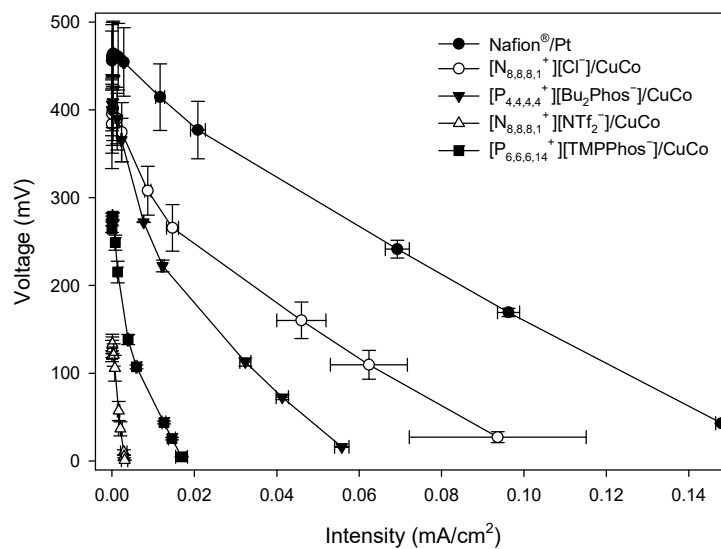**Figure A2.** Polarisation curves of MFCs with different embedded membrane-cathode assembly systems at 72 h.

Figure A3. Polarisation curves of MFCs with different embedded membrane-cathode assembly systems at 144 h.
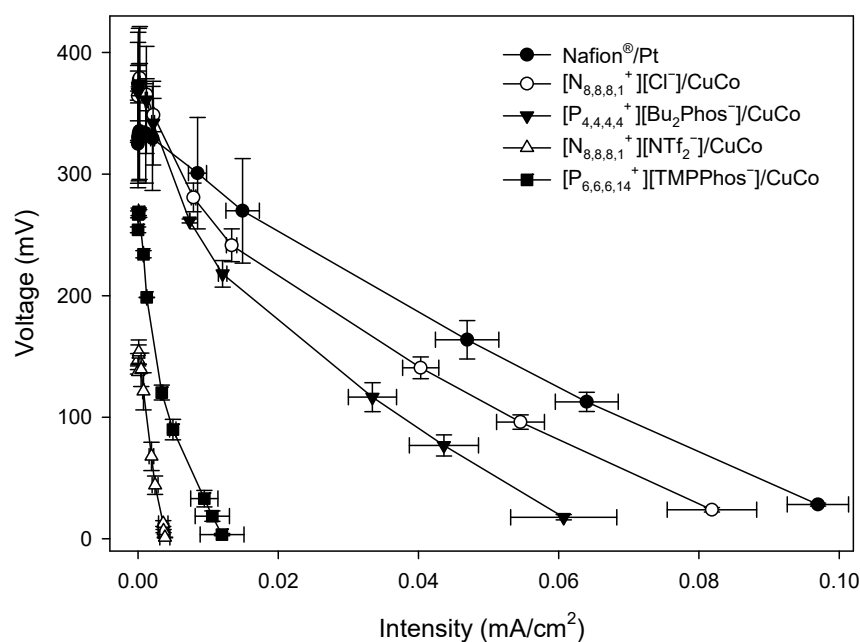
Figure A4. Polarisation curves of MFCs with different embedded membrane-cathode assembly systems at 312 h.

References

1. Marszałek, M.; Kowalski, Z.; Makara, A. Physicochemical and microbiological characteristics of pig slurry. *Tech. Trans. Chem.* **2014**, *111*, 81–91.
2. Rittmann, B.E.; McCarty, P.L. *Environmental Biotechnology: Principles and Applications*; McGraw-Hill Education: New York, NY, USA, 2001.
3. Ward, M.H.; Jones, R.R.; Brender, J.D.; de Kok, T.M.; Weyer, P.J.; Nolan, B.T. Drinking water nitrate and human health: An updated review. *Int. J. Environ. Res. Public Health* **2018**, *15*, 1557. [CrossRef] [PubMed]
4. Zonfa, T.; Kamperidis, T.; Falzarano, M.; Lyberatos, G.; Polettini, A.; Pomi, R.; Rossi, A.; Tremouli, A. Two-Stage Process for Energy Valorization of Cheese Whey through Bio-Electrochemical Hydrogen Production Coupled with Microbial Fuel Cell. *Fermentation* **2023**, *9*, 306. [CrossRef]
5. Yaqoob, A.A.; Mohamad Ibrahim, M.N.; Rafatullah, M.; Chua, Y.S.; Ahmad, A.; Umar, K. Recent Advances in Anodes for Microbial Fuel Cells: An Overview. *Materials* **2020**, *13*, 2078. [CrossRef] [PubMed]
6. Cui, Y.; Lai, B.; Tang, X. Microbial Fuel Cell-Based Biosensors. *Biosensors* **2019**, *9*, 92. [CrossRef] [PubMed]
7. Boas, J.V.; Oliveira, V.B.; Simoes, M.; Pinto, A.M.F.R. Review on microbial fuel cells applications, developments and costs. *J. Environ. Manag.* **2022**, *307*, 114525. [CrossRef]
8. Banerjee, A.; Calay, R.K.; Eregno, F.E. Role and Important Properties of a Membrane with Its Recent Advancement in a Microbial Fuel Cell. *Energies* **2022**, *15*, 444. [CrossRef]
9. Rossi, R.; Hur, A.Y.; Page, M.A.; Thomas, B.; Butkiewicz, J.J.; Jones, D.W.; Baek, G.; Saikaly, P.E.; Cropek, D.M.; Logan, B.E. Pilot scale microbial fuel cells using air cathodes for producing electricity while treating wastewater. *Water Res.* **2022**, *215*, 118208. [CrossRef]
10. Sevda, S.; Dominguez-Benetton, X.; Vanbroekhoven, K.; Wever, H.D.; Sreekrishnan, T.R.; Pant, D. High strength wastewater treatment accompanied by power generation using air cathode microbial fuel cell. *Appl. Energy* **2013**, *105*, 194–206. [CrossRef]
11. Schmidt, A.; Sturm, G.; Lapp, C.J.; Siebert, D.; Saravia, F.; Horn, H.; Ravi, P.P.; Lemmer, A.; Gescher, J. Development of a production chain from vegetable biowaste to platform chemicals. *Microb. Cell Factories* **2018**, *17*, 90. [CrossRef]
12. Roche, I.; Katuri, K.; Scotthamber, K. A microbial fuel cell using manganese oxide oxygen reduction catalysts. *J. Appl. Electrochem.* **2010**, *40*, 13–21. [CrossRef]
13. Sawant, S.Y.; Han, T.H.; Cho, M.H. Metal-Free Carbon-Based Materials: Promising Electrocatalysts for Oxygen Reduction Reaction in Microbial Fuel Cells. *Int. J. Mol. Sci.* **2017**, *18*, 25. [CrossRef] [PubMed]
14. Santoro, C.; Artyushkova, K.; Babanova, S.; Atanassov, P.; Ieropoulos, I.; Grattieri, M.; Cristiani, P.; Trasatti, S.; Li, B.; Schuler, A.J. Parameters characterization and optimization of activated carbon (AC) cathodes for microbial fuel cell application. *Bioresour. Technol.* **2014**, *163*, 54–63. [CrossRef]
15. Blázquez, E.; Gabriel, D.; Baeza, J.A.; Guisasola, A.; Ledezma, P.; Freguia, S. Implementation of a sulfide–air fuel cell coupled to a sulfate-reducing biocathode for elemental sulfur recovery. *Int. J. Environ. Res. Public Health* **2021**, *18*, 5571. [CrossRef]
16. Zhang, G.; Zhang, H.; Zhang, C.; Zhang, G.; Yang, F.; Yuan, G.; Gao, F. Simultaneous nitrogen and carbon removal in a single chamber microbial fuel cell with a rotating biocathode. *Process Biochem.* **2013**, *48*, 893–900. [CrossRef]

17. Gancarz, P.; Zorębski, E.; Dzida, M. Influence of experimental conditions on the electrochemical window. Case study on bis(trifluoromethylsulfonyl)imide-based ionic liquids. *Electrochem. Commun.* **2021**, *130*, 107107. [CrossRef]

18. Tiago, G.A.O.; Matias, I.A.S.; Ribeiro, A.P.C.; Martins, L.M.D.R.S. Application of Ionic Liquids in Electrochemistry—Recent Advances. *Molecules* **2020**, *25*, 5812. [CrossRef]

19. Ortiz-Martínez, V.M.; Ortiz, A.; Fernández-Stefanuto, V.; Tojo, E.; Colpaert, M.; Améduri, B.; Ortiz, I. Fuel cell electrolyte membranes based on copolymers of protic ionic liquid [HSO₃-BVIm][TfO] with MMA and hPFSVE. *Polymer* **2021**, *179*, 121583. [CrossRef]

20. Elhenawy, S.; Khraisheh, M.; AlMomani, F.; Al-Ghouti, M.; Hassan, M.K. From Waste to Watts: Updates on Key Applications of Microbial Fuel Cells in Wastewater Treatment and Energy Production. *Sustainability* **2022**, *14*, 955. [CrossRef]

21. Clauwaert, P.; Rabaey, K.; Aelterman, P.; De Schamphelaire, L.; Pham, T.H.; Boeckx, P.; Boon, N.; Verstraete, W. Biological denitrification in microbial fuel cells. *Environ. Sci. Technol.* **2007**, *41*, 3354–3360. [CrossRef]

22. Blázquez, E.; Gabriel, D.; Baeza, J.A.; Guisasola, A. Treatment of high-strength sulfate wastewater using an autotrophic biocathode in view of elemental sulfur recovery. *Water Res.* **2016**, *105*, 395–405. [CrossRef] [PubMed]

23. Fang, C.; Min, B.; Angelidaki, I. Nitrate as an oxidant in the cathode chamber of a microbial fuel cell for both power generation and nutrient removal purposes. *Appl. Biochem. Biotechnol.* **2010**, *164*, 464–474. [CrossRef] [PubMed]

24. Drewnowski, J.; Fernandez-Morales, F.J. Heterotrophic anodic denitrification in microbial fuel cells. *Sustainability* **2016**, *8*, 561. [CrossRef]

25. Zhang, Y.; Xu, Q.; Huang, G.; Zhang, L.; Liu, Y. Effect of dissolved oxygen concentration on nitrogen removal and electricity generation in self pH-buffer microbial fuel cell. *Int. J. Hydrogen Energy* **2020**, *45*, 34099–34109. [CrossRef]

26. Missoun, F.; de los Ríos, A.P.; Ortiz-Martínez, V.; Salar-García, M.J.; Hernández-Fernández, J.; Hernández-Fernández, F.J. Discovering Low Toxicity Ionic Liquids for Saccharomyces cerevisiae by Using the Agar Well Diffusion Test. *Processes* **2020**, *8*, 1163. [CrossRef]

27. Kebaili, H.; Pérez de los Ríos, A.; Salar García, M.J.; Ortiz-Martínez, V.M.; Kameche, M.; Hernández-Fernández, J.; Hernández-Fernández, F.J. Evaluating the Toxicity of Ionic Liquids on *Shewanella* sp. for Designing Sustainable Bioprocesses. *Front. Mater.* **2020**, *7*, 578411. [CrossRef]

28. Cong, H.N.; El Abbassi, K.; Chartier, P. Electrocatalysis of Oxygen Reduction on Polypyrrole/Mixed Valence Spinel Oxide Nanoparticles. *J. Electrochem. Soc.* **2002**, *149*, A525. [CrossRef]

29. Ortiz-Martínez, V.M.; Salar-García, M.J.; Touati, K.; Hernández-Fernández, F.J.; de los Ríos, A.P.; Belhoucine, F.; Berrabbah, A.A. Assessment of spinel-type mixed valence Cu/Co and Ni/Co-based oxides for power production in single-chamber microbial fuel cells. *Energy* **2016**, *113*, 1241–1249. [CrossRef]

30. Pujiastuti, S.; Onggo, H. Effect of various concentration of sulfuric acid for Nafion membrane activation on the performance of fuel cell. *AIP Conf. Proc.* **2016**, *1711*, 060006.

31. Kiely, P.D.; Cusick, R.; Call, D.F.; Selembo, P.A.; Regan, J.M.; Logan, B.E. Anode microbial communities produced by changing from microbial fuel cell to microbial electrolysis cell operation using two different wastewaters. *Bioresour. Technol.* **2011**, *102*, 388–394. [CrossRef]

32. Larrosa-Guerrero, A.; Scott, K.; Katuri, K.P.; Godinez, C.; Head, I.M.; Curtis, T. Open circuit versus closed circuit enrichment of anodic biofilms in MFC: Effect on performance and anodic communities. *Appl. Microbiol. Biotechnol.* **2010**, *87*, 1699–1713. [CrossRef] [PubMed]

33. Angosto, J.M.; Fernández-López, J.A.; Godínez, C. Brewery and liquid manure wastewaters as potential feedstocks for microbial fuel cells: A performance study. *Environ. Technol.* **2015**, *36*, 68–78. [CrossRef] [PubMed]

34. Hoang, A.T.; Nižetić, S.; Ng, K.H.; Papadopoulos, A.M.; Le, A.T.; Kumarf, S.; Hadiyanto, H.; Pham, V. Microbial fuel cells for bioelectricity production from waste as sustainable prospect of future energy sector. *Chemosphere* **2022**, *287*, 32285. [CrossRef] [PubMed]

35. Yaqoob, A.A.; Khatoon, A.; Mohd Setapar, S.H.; Umar, K.; Parveen, T.; Mohamad Ibrahim, M.N.; Ahmad, A.; Rafatullah, M. Outlook on the Role of Microbial Fuel Cells in Remediation of Environmental Pollutants with Electricity Generation. *Catalysts* **2020**, *10*, 819. [CrossRef]

36. Pandit, S.; Savla, N.; Sonawane, J.M.; Sani, A.M.; Gupta, P.K.; Mathuriya, A.S.; Rai, A.K.; Jadhav, D.A.; Jung, S.P.; Prasad, R. Agricultural Waste and Wastewater as Feedstock for Bioelectricity Generation Using Microbial Fuel Cells: Recent Advances. *Fermentation* **2021**, *7*, 169. [CrossRef]

37. Yokoyama, H.; Ohmori, H.; Ishida, M.; Waki, M.; Tanaka, Y. Treatment of cow-waste slurry by a microbial fuel cell and the properties of the treated slurry as a liquid manure. *Anim. Sci. J.* **2006**, *77*, 634–638. [CrossRef]

38. Larrosa, A.; Lozano, L.J.; Katuri, K.P.; Head, I.; Scott, K.; Godinez, C. On the repeatability and reproducibility of experimental two-chambered microbial fuel cells. *Fuel* **2009**, *88*, 1852–1857. [CrossRef]

39. Tomás-Alonso, F.; Rubio, A.M.; Álvarez, R.; Ortuño, J.A. Dynamic Potential Response and SEM-EDX Studies of Polymeric Inclusion Membranes Based on Ionic Liquids. *Int. J. Electrochem. Sci.* **2013**, *8*, 4955–4969. [CrossRef]